

Enhancing Person Re-Identification via Uncertainty Feature Fusion and Wise Distance Aggregation

Quang-Huy Che^{a,b,c,*}, Le-Chuong Nguyen^{b,c,*}, Vinh-Tiep Nguyen^{a,b,c,**}

^a*Multimedia Communications Laboratory*

^b*University of Information Technology, Ho Chi Minh City, Vietnam*

^c*Vietnam National University, Ho Chi Minh City, Vietnam.*

Abstract

The quest for robust Person re-identification (Re-ID) systems capable of accurately identifying subjects across diverse scenarios remains a formidable challenge in surveillance and security applications. This study presents a novel methodology that significantly enhances Person Re-Identification (Re-ID) by integrating Uncertainty Feature Fusion (UFFM) with Wise Distance Aggregation (WDA). Tested on benchmark datasets - Market-1501, DukeMTMC-ReID, and MSMT17 - our approach demonstrates substantial improvements in Rank-1 accuracy and mean Average Precision (mAP). Specifically, UFFM capitalizes on the power of feature synthesis from multiple images to overcome the limitations imposed by the variability of subject appearances across different views. WDA further refines the process by intelligently aggregating similarity metrics, thereby enhancing the system's ability to discern subtle but critical differences between subjects. The empirical results affirm the superiority of our method over existing approaches, achieving new performance benchmarks across all evaluated datasets. Code is available on Github.

Keywords: Person re-identification, Uncertainty Feature Fusion, Wise Distance Aggregation

1. Introduction

The aim of person re-identification (Re-ID) is to accurately recognize individuals across various non-overlapping camera views, a pivotal task in large-scale surveillance systems. Person Re-ID is challenged by several factors, including cluttered backgrounds, variable lighting, changes in posture, and obstructions, which commonly hinder identification. Specifically, an individual may be captured by multiple cameras within these systems, appearing across different frames as they move. Traditional retrieval solutions predominantly employ deep metric learning, wherein models are rigorously trained to convert images into vector representations. This training ensures that samples from the same category closely resemble each other in the vector space. In the querying phase, the distance between the query vector and all vectors in the database is computed, allowing for the retrieval of the most similar objects based on these distances. ReID has captured increasing attention within the computer vision community, owing to

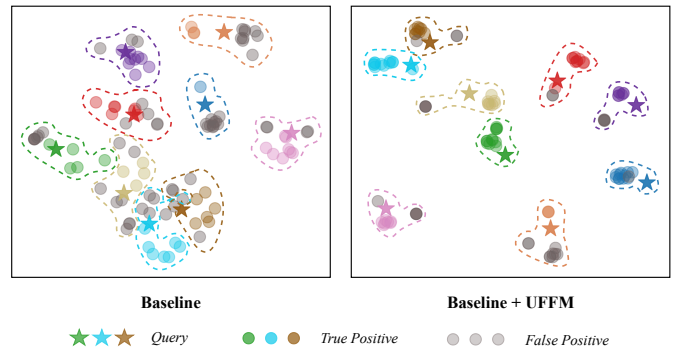


Figure 1: t-SNE visualization of image features [1]. Seven individuals from the DukeMCMT-ReID dataset are randomly selected for querying and are represented by different colors. Within a cluster comprising the top 20 query results, pentagons indicate the query images, dots of the same color as the pentagons represent correct query results, while gray dots indicate incorrect results.

*First two authors contribute equally.

**Corresponding author.

Email addresses: huycq@uit.edu.vn (Quang-Huy Che),
21520655@gm.uit.edu.vn (Le-Chuong Nguyen),
tiepvn@uit.edu.vn (Vinh-Tiep Nguyen)

its significance for video surveillance and the diverse methodologies proposed in recent times. A distinctive feature of ReID is the acquisition of images from multiple cameras, which introduces significant intra-class variance and a high degree of inter-class distance. Despite the considerable progress achieved through deep learning and large-scale public datasets, ReID remains a challenging task.

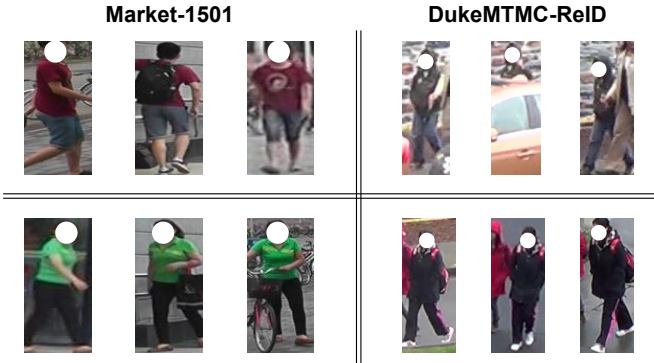


Figure 2: Examples of images of the same individual from different camera angles in the Market-1501 and DukeMTMC-ReID datasets.

To enhance ReID efficacy, recent studies have optimized the learned feature embedding space and corresponding distance metrics using two concurrent methodologies: representation learning [2, 3, 4] and metric learning [5, 6, 7]. In essence, these methodologies generate a unique representation for each image to facilitate distance computations. However, this approach is inherently limited as the features may only encapsulate specifics of that particular image. Consequently, in situations involving different poses, camera angles, or occlusions, objects belonging to the same class may exhibit low distance. The disparity in the display areas of images captured from different camera views means that certain view-specific signals generated in one image may not be present in another, despite both images depicting the same subject. More specifically, a query image captured from a pedestrian’s front might be assigned a high distance to the front view of a different pedestrian wearing a similar color outfit, rather than to an image of the queried individual taken from behind, possibly carrying a backpack. This challenge is depicted in several examples in Figure 2. Therefore, the detailed features extracted from images are not robust in ReID tasks involving subjects captured from varying angles.

In ReID problems, the representation of an object through multiple images has prompted researcher [7] to investigate the use of class-specific images to identify a representative image. This strategy shifts emphasis from the specific attributes of individual objects to more generalized features that represent the

object across various images. Despite the novelty of this method, identifying a representative for images within the same class for synthesis poses a significant challenge. The difficulty stems from collecting images through different cameras, complicating the process of identifying which images pertain to the same subject, thereby complicating the determination of a class representative. This challenge emphasizes the need for advanced methods capable of enhancing the effectiveness of techniques to identify representative individuals for each class in Re-ID tasks. This, in turn, facilitates the exploitation of specific features and general representations of the subject based on images captured from different cameras.

The utilization of images of the subject provides detailed features after extraction by the ReID model, while generalized features from the representative images of the same class convey traits from various perspectives. Employing each type of feature presents advantages and compromises when computing the distance to the feature of the query image. This introduces a research avenue on how to combine distances to leverage their benefits optimally. A straightforward integration of distances [8, 9, 10] can be achieved by directly summing the similarities or manually assigning weights during the aggregation process. However, this simplistic approach does not always yield effective results in complex scenarios. Strategically selecting weights for aggregation to optimize efficiency theoretically can harness the strengths of various methodologies.

In summary, the contributions of this paper are as follows:

- We introduce the Uncertainty Feature Fusion Method (UFFM), a novel approach to feature synthesis that does not require labeled data for objects within the same class.
- We propose the Wise Distance Aggregation method, capable of integrating various distances, including those from detailed features and generalized features, to capitalize on their strengths.
- We demonstrate that our methods achieves state-of-the-art performance on multiple person ReID datasets.

The rest of the article is presented as follows: We review related methodologies in Section 2 to understand the advantages and limitations in Person ReID tasks. Our approach includes two main contributions: the Uncertainty Feature Fusion Method (UFFM) and Wise Distance Aggregation (WDA), which are detailed in Section 3. In Section 4, we evaluate our proposals on Person ReID datasets including Market-1501, DukeMTMC-ReID, and MSMT17. In the final Section

5, we draw some conclusions and suggest directions for future research.

2. Related Work

2.1. Person Re-Identification

In the rapidly advancing context of Convolutional Neural Networks (CNNs), underscored by landmark achievements on ImageNet, ResNet-50 [11] has swiftly emerged as the architecture of choice for research and applications in the field of person re-identification (ReID), as widely recognized in numerous studies [12, 13]. The advent of the CLIP-ReID model [14], leveraging the ResNet-50 encoder from CLIP [15] instead of relying on pre-training on ImageNet, has set new benchmarks for tackling ReID challenges through a bifurcated approach aimed at enhancing the quality of visual representation. In the pursuit of exploiting local feature utilization, the study on the PCB model [2] offered profound insights into segmenting the feature map into horizontal partitions to effectively capture local features. Concurrently, initiatives such as SAN [3] and TBE-Net [4] have underscored the advantage of amalgamating both local and global features to augment identification performance. Despite the effective re-identification of individuals across disparate cameras by previous models, challenges in image identification amidst obstructions prompted the introduction of specialized modules aimed at distinguishing between body parts and personal belongings, thereby augmenting recognition capability in complex scenarios [16, 17]. Moreover, the deployment of a teacher-student framework in select studies [18, 19, 20] as a pivotal strategy has proven efficacious in refining deep learning processes, thereby elevating the precision and efficiency of object re-identification models. Additionally, the genesis of innovative loss functions [5][6] has played a crucial role in facilitating the convergence of identical ID features, enabling efficient adaptation across a spectrum of ReID models. Advanced data sampling methods, such as OfM [21] and QACConv-GS [22], have markedly improved the generalization capability and efficiency of the deep learning process, optimizing training methodologies and elevating the accuracy of ReID models.

Existing methodologies primarily focus on enhancing the model’s feature extraction capability for individual objects without harnessing the potential of combining features from multiple objects to create a composite feature rich in information. In this vein, research [7] proposed utilizing the class centroid by averaging the features of all objects within a class to represent the collective features of that class. Although this approach has proven effective in terms of query time and accuracy, the task of identifying which objects from different cameras belong to a single class poses a significant

challenge in re-identification scenarios involving images captured from diverse cameras. Conversely, another body of research [23] suggested generating multi-view features by integrating features from several fixed cameras. This proposed method employs a Graph Neural Network (GNN) to identify neighboring features without necessitating the labels of objects belonging to the same class. However, while proposing a method for synthesizing multi-view features to enhance accuracy, the algorithmic implementation inadvertently incorporates information from the query object’s camera, contravening the cross-view matching setting.

In this study, we propose a novel method to synthesize features without the prerequisite of label information of objects during the synthesis process. Moreover, our synthesis method can be seamlessly applied to pre-trained models without necessitating re-training. This attribute renders our method highly applicable in real-world scenarios, extending its utility across various domains.

2.2. Similarity aggregation

Integrating diverse similarity measures enhances re-identification accuracy by leveraging the strengths of individual similarity measures. In the study by [10], the integration of similarity metrics from various image features for content-based image retrieval was predicated on the premise that synthesizing information from multiple sources could more accurately reflect the semantic similarity between images. The research [24] proposed combining cosine similarity and Earth Mover’s Distance (EMD) [8] for face recognition, employing a two-stage process where initial cosine distance filters faces, followed by EMD ranking on the top \mathbf{K} filtered results. This method improved recognition accuracy, particularly with non-uniform face distributions. VOC-ReID [9] introduced orientation and camera-based adjustments to refine vehicle ReID, utilizing manual weight adjustments through experimentation, demonstrating efficacy despite potential optimization issues. However, a limitation of these approaches is the manual selection of combination weights, which cannot optimize combined performance optimally. In 2023, Q. Huy et al. [25] proposed combining cosine similarity with the Centroid measure [7] in the task of face recognition. Instead of manually selecting combination weights, the study proposed using feature division by triplets and incorporating a machine learning model to generate combination weights. While this approach yielded some promising initial results, the analysis within the study remained underexplored, leaving the applicability to the re-identification problem unclear. In this study, we elucidate the potential of combining features in the re-identification task, introducing a method we term Wise Similarity Aggregation (WSA).

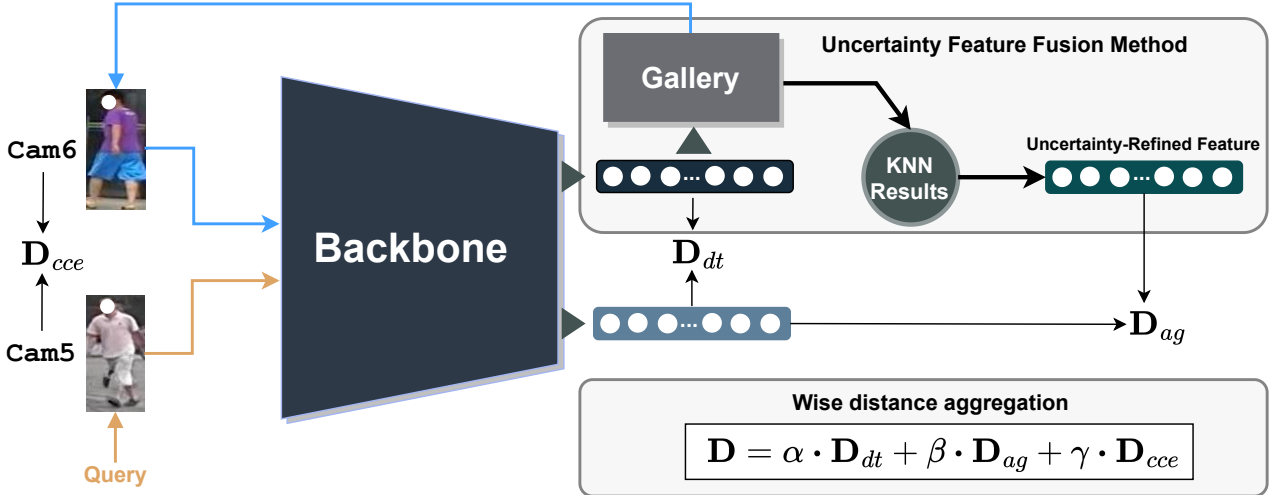


Figure 3: The process of calculating the distance between a query object and an object in the gallery. The query object is captured at Camera 5, while the object in the gallery is captured at Camera 6. Both objects are extracted through a common backbone to calculate the distance D_{dt} . Subsequently, the feature of the object in the gallery is subjected to the Uncertainty Feature Fusion Method to compute the Uncertainty-Refined Feature. Using the newly calculated Uncertainty-Refined Feature and the Detailed Feature of the query object, we calculate D_{ag} . By combining D_{dt} , D_{ag} , and D_{ccc} information of both objects, we apply the WDA method to aggregate distances.

3. Proposed Method

The proposed components of our work, when integrated with the ReID model, are depicted in Figure 3. My primary contributions include the Uncertainty Feature Fusion Method (UFFM) and Wise Distance Aggregation (WDA), both of which are involved only in the execution process of the ReID model without affecting its training phase. The Uncertainty Feature Fusion Method will be discussed in greater detail in Section 3.1, while Section 3.2 focuses on explaining the Wise Distance Aggregation method.

3.1. Uncertainty Feature Fusion Method (UFFM)

Our methodology adeptly fuses diverse features by leveraging analogous characteristics. Directly synthesizing features from the same category into a novel composite feature presents challenges, as it requires navigating the absence of additional labels for images sourced from multiple cameras. Therefore, our strategy capitalizes on the distribution within the learned embedding space to fuse features effectively. Under the assumption that the model is adeptly trained, patterns with identical identifying features will be clustered together, while those with disparate identifying features will be distinctly segregated. This proposed is termed Uncertainty Feature Fusion Method (UFFM), aligning with scientific discourse for enhanced clarity and precision.

We utilize the feature extractor E_{Θ} , trained on the dataset D_{train} , to map an image I to a vector $f \in \mathbb{R}^d$, $f = E_{\Theta}(I)$. Utilizing f , we identify the K -nearest neighbors, denoted as $F^{nn} = \{f_k^{nn}\}_{k=1}^K$, where each $f_k^{nn} \in \mathbb{R}^d$. Although the selection of K is unsupervised, an optimally structured embedding space will still exhibit neighboring instances within the same class as f . In this case, incorrect results may introduce noise to the fusion features, but correct results will enhance the information in the fusion features, as shown in Figure 4. To fuse features from neighboring features, a simple averaging approach is not always effective due to variability in distance between f and f_k^{nn} . Therefore, we advocate for a weighted synthesis approach, where distance play a crucial role in determining the contribution of each neighbor to the composite feature. Leveraging the list of K -nearest neighbors F^{nn} , we generate a corresponding list of cosine distances.

$$\mathbf{D}^{nn} = \{d_k^{nn}\}_{k=1}^K, \quad d_k^{nn} = dst(f, f_k^{nn}) \quad (1)$$

Upon obtaining the distance list \mathbf{D}^{nn} , weights are computed in relation to each distance, thereby delineating the contribution level of neighboring features into our feature synthesis process. The equation below elucidates the method of merging features based on their assigned weights, where Uncertainty-Refined Feature, f^{URF} represents the fusion feature based on f :

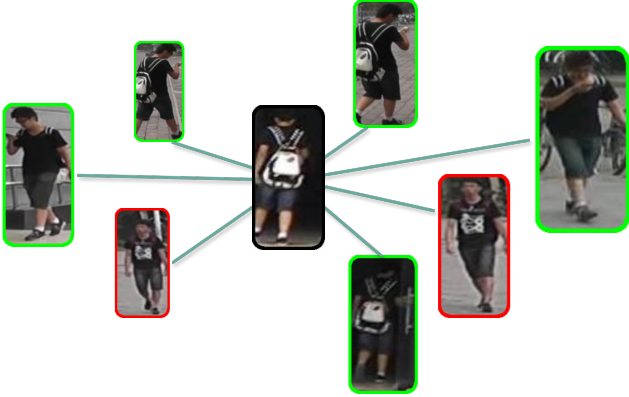


Figure 4: An example of finding K nearest neighbors based on features, with $K=7$. The black box represents the query object, green boxes indicate correct results, while red boxes denote incorrect results.

$$f^{URF} = \sum_{k=1}^K w_k \cdot f_k^{nn}, \quad w_k = \frac{d_i^{nn}}{\sum_{i=1}^K d_i^{nn}} \quad (2)$$

This ensures that the contribution of each neighboring feature is proportionate to its distance to f , facilitating a weighted synthesis that captures the most relevant and significant features from the nearest neighbors.

In the evaluation phase of most Re-Identification (ReID) problems, the cross-view matching setting is commonly applied. Initially, we define $\mathcal{Q} = \{q_i\}_{i=1}^{N_q}$ and $\mathcal{G} = \{g_j\}_{j=1}^{N_g}$ as the query set and the gallery set, respectively. Traditionally, for a query q_i , it is required to compute the distances with each $g_j \in \mathcal{G}$ to obtain a distance list $List(q_i, \mathcal{G}) = \{\mathbf{D}_{dt}(q_i, g_j)\}_{j=1}^{N_g}$. Then, $List(q_i, \mathcal{G})$ is sorted, excluding objects with both the same ID and camera from the result list. This implies that valid results are those captured by a different camera than that of the query. To ensure the cross-view matching setting in the feature synthesis process with our method, we address this by selecting only the K features captured by a different camera than that of the feature under consideration, or $\text{Camera}(f_i^{nn}) \neq \text{Camera}(f)$. This approach ensures that the fusion feature does not carry the characteristics of the query, thus maintaining fairness when using the cross-view matching setting in the evaluation process. After applying the Uncertainty Feature Fusion Method (UFFM) method on each g_j in the gallery set, resulting in $List(q_i, \mathcal{G}) = \{\mathbf{D}_{ag}(q_i, g_j)\}_{j=1}^{N_g}$.

3.2. Wise Distance Aggregation

In multi-view camera systems, feature usage has proven effective for generalizing and consistently identifying object characteristics across varied observational

environments. However, this method’s significant limitation is its potential to overlook complex image details, thereby impeding the accurate and comprehensive identification of an object’s unique attributes. To address this challenge, this study introduces an advanced technique aimed at synthesizing and optimizing information from two types of distances: distance to Detailed Feature (\mathbf{D}_{dt}) and distance to Uncertainty-Refined Feature (\mathbf{D}_{ag}). Rather than manually combining features with predetermined weights, we propose an intelligent method for aggregating distances, utilizing the cosine distance metric, which ranges from -1 to 1. The expected form of the aggregated distance is:

$$\mathbf{D} = \alpha \cdot \mathbf{D}_{dt} + \beta \cdot \mathbf{D}_{ag} \quad (3)$$

We define \mathbf{D}_{dt} and \mathbf{D}_{ag} as inputs for the Linear Regression model, with the expected output being 1 if the IDq_i matches IDg_j and -1 otherwise. We generate data for the linear regression model by randomly selecting triplets: anchor (x_a), positive (x_p), and negative (x_n). For each pair (x_a v \grave{a} x_p), we create a data point for the training set labeled as 1, and for (x_a v \grave{a} x_n), labeled as -1. After training, the model take the form similar to Equation 4.

$$\mathbf{D} = w_2 \cdot \mathbf{D}_{dt} + w_1 \cdot \mathbf{D}_{ag} + w_0 \quad (4)$$

where, w_2 v \grave{a} w_1 denote the weights assigned to two types of distances. This approach facilitates the integration of the strengths associated with different distances. The detailed procedure is elaborated in Algorithm 1. To maintain independence during the evaluation phase, only the training dataset \mathbf{D}_{train} , which includes known IDs for images from distinct cameras, is utilized in the data preparation process. Rather than employing uncertain feature fusion method to generate the uncertainty-refined feature f^{URF} within the D_{train} dataset, which encompasses IDs for subjects observed through various cameras. This research exploits the available data to fuse multi-view features via a method referred to as Certain Feature Fusion Method (CFFM), where Refined Feature, f^{RF} is delineated in Equation 5. With $F^{cnn} = \{f_k^{cnn}\}_{k=1}^K$ being the set of features that are most similar to f and of the same class as f . This ensures that the features within F^{cnn} are of the same class as f .

$$f^{RF} = \frac{1}{K} \sum_{k=1}^K f_k^{cnn} \quad (5)$$

Furthermore, to enhance the distinctiveness of features derived from different camera views, we adapt the Cross-Camera Encouragement (CCE) technique, initially proposed by Lin et al. [30], modifying its application to better suit our methodology. The revised CCE

Table 1: Comparison of our method with person ReID SOTA methods. The best and second best results are marked in **bold** and underline respectively.

Methods	Market-1501		DukeMTMC-ReID		MSMT17	
	Rank@1	mAP	Rank@1	mAP	Rank@1	mAP
BoT [12] (WCVPR'19)	94.5	85.9	86.4	76.4	74.1	50.2
CLIP-ReID Baseline [14] (AAAI'22)	94.7	88.1	88.6	79.3	82.1	60.7
ISP [16] (ICCV'20)	-	-	88.7	78.9	-	-
HG [18] (BMVC'21)	95.6	86.1	87.1	77.5	-	-
PAT [26] (CVPR'21)	95.4	88.0	88.8	78.2	-	-
CAL [27] (ICCV'21)	94.5	87.0	87.2	76.4	79.5	56.2
OfM [21] (AAAI'21)	94.9	87.9	89.0	78.6	-	-
MGN+CircleLoss [5] (AAAI'21)	<u>96.1</u>	87.4	-	-	76.9	52.1
DRL-Net [28] (TMM'22)	94.7	86.9	88.1	76.6	78.4	55.3
QAConv-GS [22] (CVPR'22)	91.6	75.5	-	-	79.1	49.5
CLIP-ReID [14] (AAAI'22)	95.7	89.8	90.0	<u>84.7</u>	84.4	<u>63.0</u>
AGW [29] (TPAMI'22)	95.1	87.8	89.0	79.6	68.3	49.3
FastReID [13] (ACM MM'23)	95.4	88.2	89.6	79.8	83.3	59.9
BPBreID [17] (WACV'23)	95.1	87.0	89.6	78.3	-	-
BoT + Our	96.2	<u>91.0</u>	<u>90.3</u>	83.1	82.0	62.3
CLIP-ReID Baseline + Our	<u>96.1</u>	92.0	91.3	85.0	<u>83.8</u>	67.6

formula is integrated into our composite distance calculation, thereby enriching the feature discrimination capability essential for reliable object re-identification:

$$\mathbf{D}_{cce} = CCE(x_a, x_b) = \begin{cases} 1, & c_a = c_b \\ 0, & c_a \neq c_b \end{cases} \quad (6)$$

To align with our methodological approach more closely, we incorporate \mathbf{D}_{cce} into the composite distance calculation, which can be substituted in the detailed distance formula as seen in Equation 3:

$$\mathbf{D} = \alpha \cdot \mathbf{D}_{dt} + \beta \cdot \mathbf{D}_{ag} + \gamma \cdot \mathbf{D}_{cce} \quad (7)$$

At this juncture, the aggregate distance can be optimized through the employment of a Linear Regression model, as delineated in Equation 4 with (α, β, γ) are weight of model.

4. Experimental Results

4.1. Datasets and Settings

4.1.1. Datasets

We conducted training and evaluation of the proposed model on three Person ReID datasets: Market1501[31], DukeMTMC-ReID[32] and MSMT17[33]:

- Market-1501[31]: The Market-1501 dataset was collected using six cameras positioned in front of a

Algorithm 1: Triplet Data Generation Algorithm

Input: $N \geq 0$; // Number of iterations

//Initialization step

$i \leftarrow 1$;

$D_{\text{train}} \leftarrow \emptyset$;

//Loop to prepare data

for $i \leftarrow 1$ **to** N **do**

 //Extract feature step

$x_a, x_p, x_n \leftarrow D_{\text{train}}$;

$f_a, f_p, f_n \leftarrow E_{\Theta}(x_a, x_p, x_n)$;

 //Prepare positive data

$f_p^{RF} \leftarrow \text{CFFM}(f_p)$;

$\mathbf{D}_{dt}^p \leftarrow \text{dst}(f_a, f_p)$;

$\mathbf{D}_{ag}^p \leftarrow \text{dst}(f_a, f_p^{RF})$;

$\mathbf{D}_{cce}^p \leftarrow \text{CCE}(x_a, x_p)$;

 //Prepare negative data

$f_n^{RF} \leftarrow \text{CFFM}(f_n)$;

$\mathbf{D}_{dt}^n \leftarrow \text{dst}(f_a, f_n)$;

$\mathbf{D}_{ag}^n \leftarrow \text{dst}(f_a, f_n^{RF})$;

$\mathbf{D}_{cce}^n \leftarrow \text{CCE}(x_a, x_n)$;

 //Put the data into the training set of the model

$D_{\text{train}} \leftarrow D_{\text{train}} \cup \left\{ \left[\mathbf{D}_{dt}^p, \mathbf{D}_{ag}^p, \mathbf{D}_{cce}^p \right], 1 \right\}$;

$D_{\text{train}} \leftarrow D_{\text{train}} \cup \left\{ \left[\mathbf{D}_{dt}^n, \mathbf{D}_{ag}^n, \mathbf{D}_{cce}^n \right], -1 \right\}$;

Table 2: Evaluation of our proposed methods with BoT Baseline and CLIP-ReID Baseline

Baseline	UFFM	WDA	Market-1501		DukeMTMC-ReID		MSMT17	
			Rank@1	mAP	Rank@1	mAP	Rank@1	mAP
BoT Baseline	✓	---	94.5	85.9	86.4	76.4	74.1	50.2
			96.1	91.2	90.2	83.3	81.5	61.8
	↑ 1.6	↑ 5.3	↑ 3.8	↑ 6.9	↑ 7.4	↑ 11.6		
	✓	✓	96.2 \pm 0.05	91.0 \pm 0.1	90.3 \pm 0.09	83.1 \pm 0.13	82.0 \pm 0.24	62.3 \pm 0.3
			↑ 1.7	↑ 5.1	↑ 3.9	↑ 6.7	↑ 7.9	↑ 12.1
CLIP-ReID Baseline	✓	---	94.7	88.1	88.6	79.3	82.1	60.7
			95.7	92.0	90.7	84.8	83.4	67.7
	↑ 1.0	↑ 3.9	↑ 2.1	↑ 5.5	↑ 1.3	↑ 7.0		
	✓	✓	96.1 \pm 0.13	92.0 \pm 0.05	91.3 \pm 0.45	85.0 \pm 0.18	83.8 \pm 0.36	67.6 \pm 0.55
			↑ 1.4	↑ 3.9	↑ 2.7	↑ 5.7	↑ 1.7	↑ 6.9

supermarket at Tsinghua University. It comprises a total of 32,668 images belonging to 1,501 individuals. The dataset is divided into 12,936 training images with 751 individuals and 19,732 testing images with 750 individuals. Among the test images, 3,368 are selected as the query set.

- DukeMTMC-ReID[32]: The DukeMTMC-ReID dataset, a subset of DukeMTMC, is tailored for image-based person re-identification. Captured from high-resolution videos by eight cameras, it’s a significant pedestrian image dataset. Images are meticulously cropped using hand-drawn bounding boxes. It comprises 16,522 training images covering 702 identities, 2,228 query images of the other 702 identities and 17,661 gallery images.
- MSMT17[33]: MSMT17 is a comprehensive multi-scene multi-time person re-identification dataset. It includes 180 hours of video footage captured by 12 outdoor cameras and 3 indoor cameras across 12 different time slots. With 4,101 annotated identities and 126,441 bounding boxes, it offers extensive data for re-identification research.

4.1.2. Implementation Details

In this study, we utilize a Baseline model derived from BoT [12] and CLIP-ReID Baseline [14], employing a ResNet50 architecture as its backbone. Our methodology leverages readily available pretrained models, eliminating the necessity for retraining. We standardize the dimensions of all images to 256×128 for the inference process. For the UFFM approach, we select a coefficient of $K=4$ for Market-1501 and DukeMTMC-ReID, and $K=6$ for MSMT17. For the results obtained by integrating the WDA, we conducted the algorithm five times to ensure fairness, due to the random nature of the Triplet Data Generation Algorithm. The results presented are the mean of these five runs. All

experiments were conducted using the PyTorch framework on an NVIDIA GeForce RTX 4090 GPU, equipped with 32GB of RAM, and powered by an Intel® Core™ i9-10900X CPU.

4.2. Comparison with Person ReID State-of-the-Art Methods

In our study, we benchmark our method against other person ReID approaches, as detailed in Table 1. This table provides an in-depth comparison of the performance of various methods across three standard datasets in person re-identification: Market-1501, DukeMTMC-ReID, and MSMT17. Our comparison primarily focuses on methods that employ a ResNet50 backbone and resize images to 256×128 . The evaluation metrics, Rank-1 accuracy (Rank@1) and mean Average Precision (mAP), serve as crucial benchmarks for assessing the effectiveness of these methods in person re-identification tasks.

As depicted in Table 1, the integration of our approach with the CLIP-ReID Baseline not only achieves the highest performance metrics, recording an mAP of 92.0% and Rank-1 accuracy of 96.1% on Market-1501, as well as an mAP of 85.0% and Rank-1 accuracy of 91.3% on DukeMTMC-ReID, but also showcases remarkable results on MSMT17 with an mAP of 67.6% and Rank-1 accuracy of 83.8%. When applied in conjunction with BoT, another foundational model in the person ReID domain, our method similarly demonstrates significant improvements, achieving a Market-1501 mAP of 91.0% and Rank-1 accuracy of 96.2%, alongside an mAP of 83.1% and Rank-1 accuracy of 90.3% on DukeMTMC-ReID. This underlines the substantial enhancement potential of our proposed method across various foundational architectures.

Notably, when compared to competitive models, and other iterations of CLIP-ReID, our method exhibits superior performance. For instance, while

Table 3: Ablation study of distance metrics using WDA on Person ReID datasets.

	WDA			Market-1501		DukeMTMC-ReID		MSMT17	
	D_{dt}	D_{ag}	D_{cce}	Rank@1	mAP	Rank@1	mAP	Rank@1	mAP
BoT Baseline	✓			94.5	85.9	86.4	76.4	74.1	50.2
		✓		96.1	91.2	90.2	83.3	81.5	61.8
	✓	✓		96.0	90.9	90.0	82.9	80.8	61.0
	✓		✓	95.6	87.3	88.8	78.7	77.5	53.6
	✓	✓	✓	96.2	91.0	90.3	83.1	82.0	62.3
CLIP-ReID Baseline	✓			94.7	88.1	88.6	79.3	82.1	60.7
		✓		95.7	92.0	90.7	84.8	83.4	67.7
	✓	✓		95.9	91.9	90.6	84.6	83.4	67.2
	✓		✓	95.4	88.8	90.5	80.8	82.2	58.7
	✓	✓	✓	96.1	92.0	91.3	85.0	83.8	67.6

MGN+CircleLoss showed strong performance with a Rank-1 accuracy of 96.1% on Market-1501, our approach with the CLIP-ReID Baseline surpasses this with both higher mAP and Rank-1 metrics. Similarly, FastReID, which is renowned for its efficiency and effectiveness, achieved a commendable Rank-1 accuracy of 83.3% on MSMT17, yet our method still outperforms it, particularly in terms of mAP. Moreover, our approach exceeds the CLIP-ReID’s own previous benchmarks, setting new standards for mAP and Rank-1 accuracy across the board. These advancements over competitive models do not merely highlight the efficacy of our proposed method but also emphasize its adaptability and scalability to diverse and complex datasets.

4.3. Ablation study

4.3.1. Effectiveness of UFFM and WDA

Table 2 demonstrate the effectiveness of our method when combined with the BoT Baseline [12] and the CLIP-ReID Baseline [14]. This table provides a detailed look at the performance improvements of our proposed methods compared to the baselines of BoT and CLIP-ReID across three prominent datasets in the field of Re-identification: Market-1501, DukeMTMC-ReID, and MSMT17. The outcomes are measured using two primary metrics: Rank@1 and mAP, both of which reflect the accuracy and reliability of the model in re-identifying identities.

For the BoT Baseline [12] on the Market-1501 dataset, we observe an improvement from 94.5% to 96.2% in Rank@1 and from 85.9% to 91.0% in mAP after applying UFFM and WDA, indicating significant performance enhancements. On the DukeMTMC-ReID, Rank@1 increased from 86.4% to 90.3%, and mAP from 76.4% to 83.1%. Meanwhile, MSMT17 saw a Rank@1 increase from 74.1% to 82.0% and mAP from 50.2% to 62.3%, marking a considerable leap in performance. The CLIP-ReID Baseline [14] also witnessed similar improvements. With Market-1501, Rank@1

Table 4: Comparison of Accuracy Using UFFM and CFFM

	Market-1501		DukeMTMC-ReID	
	Rank@1	mAP	Rank@1	mAP
UFFM	95.7	91.9	90.6	84.7
CFFM	96.1	92.0	91.3	85.0

went up from 94.7% to 96.1%, and mAP from 88.1% to 92.0%. DukeMTMC-ReID saw Rank@1 increase from 88.6% to 91.3% and mAP from 79.3% to 85.0%. The MSMT17 dataset showed a Rank@1 increase from 82.1% to 83.8% and mAP from 60.7% to 67.6%.

Although in all cases the application of UFFM+WDA results in higher Rank@1 scores than applying UFFM alone, there are instances where the mAP decreases. This suggests that while the WDA method can enhance accuracy, it may, in some cases, reduce the model’s ability to comprehensively identify results compared to using the UFFM method alone. Nevertheless, these improvements indicate that combining UFFM and WDA not only enhances accuracy but also strengthens the model’s generalization capabilities across large and complex datasets. Notably, the significant increase in mAP on MSMT17, a dataset characterized by its high difficulty and diversity, demonstrates that these methods are particularly effective in improving recognition capabilities under challenging conditions.

4.3.2. Ablation study of UFFM and CFFM

Table 4 presents the results of the Feature Fusion Methods in the Triplet Data Generation Algorithm 1. The results indicate that both Rank@1 and mAP are improved when using the CFFM method to fuse features in the Triplet Data Generation Algorithm across both the Market-1501 and DukeMTMC-ReID datasets, with a pretrained CLIP-ReID Baseline.

4.3.3. Effectiveness of different distances

Table 3 presents the performance of combining different types of distances using the Wise Distance Aggregation (WDA) method. The results indicate that combining just two types of distances-either (\mathbf{D}_{dt} and \mathbf{D}_{ag}) or (\mathbf{D}_{dt} and \mathbf{D}_{cce})-sometimes yields lower performance than using \mathbf{D}_{ag} alone. However, simultaneously integrating all three distances: \mathbf{D}_{dt} , \mathbf{D}_{ag} , and \mathbf{D}_{cce} consistently results in superior outcomes compared to using single distances or any pair of distances. This demonstrates that a judicious combination of multiple distance metrics can enhance the effectiveness of Re-ID solutions.

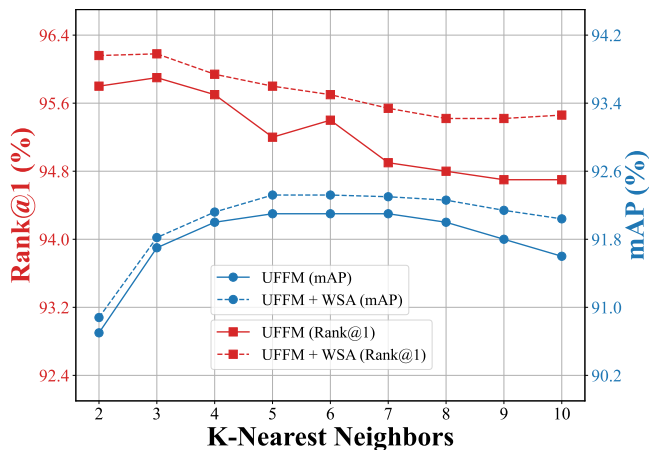


Figure 5: Market1501

4.4. Parameters analysis

Our method primarily relies on two parameters: K and n , where K directly determines the number of nearest neighbors, and n represents the number of iterations for computing weights in the WDA method. We present the impact of varying these parameters on Market-1501 dataset. The K coefficient is adjusted from 1 to 10, while n is set to range from 200 to 1000, with incremental steps of 200 for n . The metrics in Figure 6 illustrate that Rank@1 accuracy and mAP do not follow a linear trend with increasing values of K or n . Notably, with the K coefficient, there is always a trade-off between mAP and Rank@1 accuracy when varying K . We set n at 400 for both datasets when assessing accuracy changes in both UFFM and UFFM+WDA methods. Our findings, as depicted in Figure 5, indicate that both methods exhibit a trade-off between Rank@1 accuracy and mAP with different K values, and the UFFM+WDA method consistently outperforms UFFM across various K coefficients.

4.5. Visualization of results

We present visual examples of the top 10 rankings as determined by the baseline CLIP-ReID model and our proposed method in Figure 7 for the Market-1501 and DukeMTMC-ReID datasets, respectively. The results demonstrate that the baseline model struggles with query retrieval when subjects change posture or are occluded. Notably, integrating our method significantly enhances performance, effectively handling subjects in various postures within the Market-1501 dataset (Figure 7a) and achieving robust results even in scenarios where subjects are occluded in the DukeMTMC-ReID dataset (Figure 7b). These visualizations underscore the efficacy of our approach in Feature Fusion for improved re-identification.

5. Conclusion

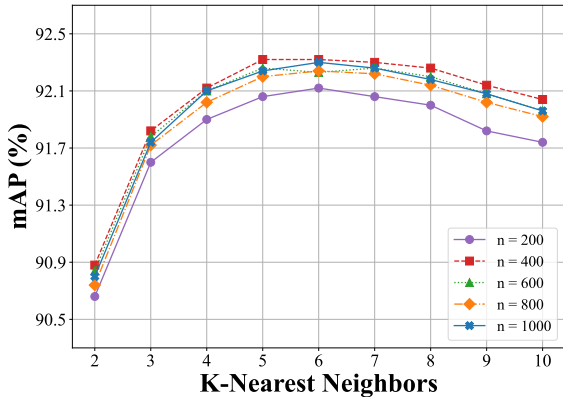
This study has introduced two advanced methodologies: Uncertainty Feature Fusion Method (UFFM) and Wise Distance Aggregation (WDA), along with their empirical evaluations on standard datasets such as Market-1501, DukeMTMC-ReID, and MSMT17. These methodologies not only enhance Rank-1 accuracy and mean Average Precision (mAP) but also effectively address challenges posed by image transformations due to varying camera angles and occlusions. The integration of UFFM and WDA provides a robust and versatile approach for person re-identification, paving new paths for the development of surveillance systems, particularly in contexts that demand high accuracy and reliability. We anticipate that these findings will make a significant contribution to the field of camera-based person identification and encourage further research in optimizing and adapting these methods to complex real-world scenarios.

6. Acknowledgement

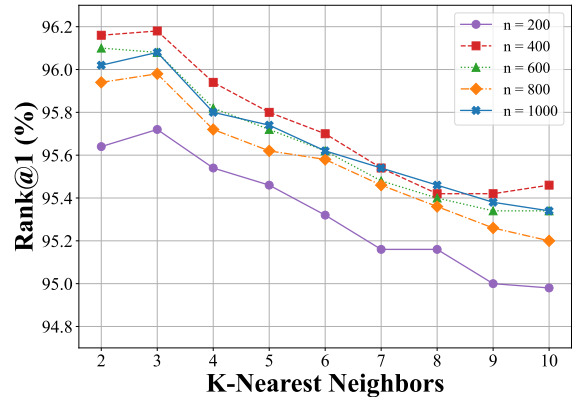
This research was supported by The VNUHC-MUniversity of Information Technology’s Scientific Research Support Fund.

References

- [1] L. van der Maaten, G. Hinton, Visualizing data using t-sne, *Journal of Machine Learning Research* 9 (2008) 2579–2605.
- [2] Y. Sun, L. Zheng, Y. Yang, Q. Tian, S. Wang, Beyond part models: Person retrieval with refined part pooling (and a strong convolutional baseline), in: V. Ferrari, M. Hebert, C. Sminchisescu, Y. Weiss (Eds.), *Computer Vision – ECCV 2018*, Springer International Publishing, Cham, 2018, pp. 501–518.
- [3] J. Qian, W. Jiang, H. Luo, H. Yu, Stripe-based and attribute-aware network: a two-branch deep model for vehicle re-identification, *Measurement Science and Technology* 31 (2019).



(a) Impact of Parameter K and n on mAP Performance



(b) Impact of Parameters K and n on Rank@1 Performance

Figure 6: Impact of Parameters K and n on Market-1501



(a) Market1501



(b) DukeMTMC-ReID

Figure 7: The results of the CLIP-ReID Baseline model are on the left and those of the CLIP-ReID Baseline combined with our method are on the right. Each row displays query images and the top 10 retrieved library images. Green and red boxes indicate true positives and false positives, respectively.

- [4] W. Sun, G. Dai, X. Zhang, X. He, X. Chen, Tbe-net: A three-branch embedding network with part-aware ability and feature complementary learning for vehicle re-identification, *IEEE Transactions on Intelligent Transportation Systems* 23 (9) (2022) 14557–14569. doi:10.1109/TITS.2021.3130403.
- [5] Y. Sun, C. Cheng, Y. Zhang, C. Zhang, L. Zheng, Z. Wang, Y. Wei, Circle loss: A unified perspective of pair similarity optimization, in: 2020 IEEE/CVF Conference on Computer Vision and Pattern Recognition (CVPR), 2020, pp. 6397–6406. doi:10.1109/CVPR42600.2020.00643.
- [6] C. Yan, G. Pang, X. Bai, C. Liu, X. Ning, L. Gu, J. Zhou, Beyond triplet loss: Person re-identification with fine-grained difference-aware pairwise loss, *IEEE Transactions on Multimedia* 24 (2022) 1665–1677. doi:10.1109/TMM.2021.3069562.
- [7] M. Wiecezorek, B. Rychalska, J. Dabrowski, On the unreasonable effectiveness of centroids in image retrieval (2021). arXiv:2104.13643.
- [8] The earth mover’s distance as a metric for image retrieval.
- [9] X. Zhu, Z. Luo, P. Fu, X. Ji, Voc-reid: Vehicle re-identification based on vehicle-orientation-camera, in: Proc. CVPR Workshops, 2020.
- [10] M. Arevalillo-Herráez, J. Domingo, F. J. Ferri, Combining similarity measures in content-based image retrieval, *Pattern Recognition Letters* 29 (16) (2008) 2174–2181. doi:https://doi.org/10.1016/j.patrec.2008.08.003. URL https://www.sciencedirect.com/science/article/pii/S0167865508002511
- [11] K. He, X. Zhang, S. Ren, J. Sun, Deep residual learning for image recognition, 2015, pp. 770–778.
- [12] H. Luo, Y. Gu, X. Liao, S. Lai, W. Jiang, Bag of tricks and a strong baseline for deep person re-identification, in: 2019 IEEE/CVF Conference on Computer Vision and Pattern Recognition Workshops (CVPRW), 2019, pp. 1487–1495. doi:10.1109/CVPRW.2019.00190.
- [13] L. He, X. Liao, W. Liu, X. Liu, P. Cheng, T. Mei, Fastreid: A pytorch toolbox for general instance re-identification, in: Proceedings of the 31st ACM International Conference on Multimedia, MM ’23, Association for Computing Machinery, New York, NY, USA, 2023, p. 9664–9667. doi:10.1145/3581783.3613460. URL https://doi.org/10.1145/3581783.3613460
- [14] S. Li, L. Sun, Q. Li, Clip-reid: Exploiting vision-language model for image re-identification without concrete text labels, in: AAAI Conference on Artificial Intelligence, 2022.
- [15] A. Radford, J. W. Kim, C. Hallacy, A. Ramesh, G. Goh, S. Agarwal, G. Sastry, A. Askell, P. Mishkin, J. Clark, G. Krueger, I. Sutskever, Learning transferable visual models from natural language supervision, in: International Conference on Machine Learning, 2021.
- [16] K. Zhu, H. Guo, Z. Liu, M. Tang, J. Wang, Identity-guided human semantic parsing for person re-identification, *ECCV* (2020).
- [17] V. Somers, C. D. Vleeschouwer, A. Alahi, Body part-based representation learning for occluded person re-identification, 2022, pp. 1613–1623.
- [18] M. Kiran, R. G. Praveen, L. T. Nguyen-Meidine, S. Belharbi, L.-A. Blais-Morin, E. Granger, Holistic guidance for occluded person re-identification, in: British Machine Vision Conference, 2021. URL https://api.semanticscholar.org/CorpusID:233231173
- [19] P. Khorramshahi, V. Shenoy, R. Chellappa, Robust and scalable vehicle re-identification via self-supervision, in: 2023 IEEE/CVF Conference on Computer Vision and Pattern Recognition Workshops (CVPRW), 2023, pp. 5295–5304. doi:10.1109/CVPRW59228.2023.00558.
- [20] X. Jin, C. Lan, W. Zeng, Z. Chen, Uncertainty-aware multi-shot knowledge distillation for image-based object re-identification, in: AAAI Conference on Artificial Intelligence, 2020.
- [21] One for more: Selecting generalizable samples for generalizable reid model 35 (2021) 3324–3332. doi:10.1609/aaai.v35i4.16444. URL https://ojs.aaai.org/index.php/AAAI/article/view/16444
- [22] S. Liao, L. Shao, Graph Sampling Based Deep Metric Learning for Generalizable Person Re-Identification (June 2022).
- [23] Y. Xu, Z. Jiang, A. Men, H. Wang, H. Luo, Multi-view feature fusion for person re-identification, *Knowledge-Based Systems* 229 (2021) 107344. doi:https://doi.org/10.1016/j.knosys.2021.107344. URL https://www.sciencedirect.com/science/article/pii/S0950705121006067
- [24] H. T. Phan, A. M. Nguyen, Deepface-emd: Re-ranking using patch-wise earth mover’s distance improves out-of-distribution face identification, 2021, pp. 20227–20237.
- [25] Q.-H. Che, H.-T. Le, M.-D. Ngo, H.-L. Tran, D.-D. Phan, Intelligent attendance system: Combining fusion setting with robust similarity measure for face recognition, in: 2023 International Conference on Multimedia Analysis and Pattern Recognition (MAPR), 2023, pp. 1–6. doi:10.1109/MAPR59823.2023.10288710.
- [26] Y. Li, J. He, T. Zhang, X. Liu, Y. Zhang, F. Wu, Diverse part discovery: Occluded person re-identification with part-aware transformer, 2021 IEEE/CVF Conference on Computer Vision and Pattern Recognition (CVPR) (2021) 2897–2906.
- [27] Y. Rao, G. Chen, J. Lu, J. Zhou, Counterfactual attention learning for fine-grained visual categorization and re-identification, in: ICCV, 2021.
- [28] M. Jia, X. Cheng, S. Lu, J. Zhang, Learning disentangled representation implicitly via transformer for occluded person re-identification, *IEEE Transactions on Multimedia* 25 (2023) 1294–1305. doi:10.1109/TMM.2022.3141267.
- [29] M. Ye, J. Shen, G. Lin, T. Xiang, L. Shao, S. H. Hoi, Deep learning for person re-identification: A survey and outlook, *IEEE Transactions on Pattern Analysis and Machine Intelligence* 44 (06) (2022) 2872–2893. doi:10.1109/TPAMI.2021.3054775.
- [30] Y. Lin, L. Xie, Y. Wu, C. C. Yan, Q. Tian, Unsupervised person re-identification via softened similarity learning, 2020 IEEE/CVF Conference on Computer Vision and Pattern Recognition (CVPR) (2020) 3387–3396.
- [31] L. Zheng, L. Shen, L. Tian, S. Wang, J. Wang, Q. Tian, Scalable person re-identification: A benchmark, in: Computer Vision, IEEE International Conference on, 2015.
- [32] E. Ristani, F. Solera, R. Zou, R. Cucchiara, C. Tomasi, Performance measures and a data set for multi-target, multi-camera tracking, in: European Conference on Computer Vision workshop on Benchmarking Multi-Target Tracking, 2016.
- [33] L. Wei, S. Zhang, W. Gao, Q. Tian, Person transfer gan to bridge domain gap for person re-identification, in: 2018 IEEE/CVF Conference on Computer Vision and Pattern Recognition, 2018, pp. 79–88. doi:10.1109/CVPR.2018.00016.